

# The macroscopic delamination of thin films from elastic substrates

Dominic Vella<sup>a,b</sup>, José Bico<sup>a</sup>, Arezki Boudaoud<sup>b</sup>, Benoit Roman<sup>a</sup>, and Pedro M. Reis<sup>c,1</sup>

<sup>a</sup>Physique et Mécanique des Milieux Hétérogènes, École Supérieure de Physique et de Chimie Industrielles, Universités Paris 6 and 7, Centre National de la Recherche Scientifique Unité Mixte de Recherche 7636, ParisTech, 10 Rue Vauquelin, 75231 Paris Cedex 05, France; <sup>b</sup>Laboratoire de Physique Statistique, École Normale Supérieure, Université Pierre et Marie Curie, Paris 06, Université Paris Diderot, Centre National de la Recherche Scientifique, 24 Rue Lhomond, 75005 Paris, France; and <sup>c</sup>Department of Mathematics, Massachusetts Institute of Technology, Cambridge, MA 02139

Edited by Harry L. Swinney, University of Texas, Austin, TX, and approved May 6, 2009 (received for review February 26, 2009)

**The wrinkling and delamination of stiff thin films adhered to a polymer substrate have important applications in “flexible electronics.” The resulting periodic structures, when used for circuitry, have remarkable mechanical properties because stretching or twisting of the substrate is mostly accommodated through bending of the film, which minimizes fatigue or fracture. To date, applications in this context have used substrate patterning to create an anisotropic substrate-film adhesion energy, thereby producing a controlled array of delamination “blisters.” However, even in the absence of such patterning, blisters appear spontaneously, with a characteristic size. Here, we perform well-controlled experiments at macroscopic scales to study what sets the dimensions of these blisters in terms of the material properties and explain our results by using a combination of scaling and analytical methods. Besides pointing to a method for determining the interfacial toughness, our analysis suggests a number of design guidelines for the thin films used in flexible electronic applications. Crucially, we show that, to avoid the possibility that delamination may cause fatigue damage, the thin film thickness must be greater than a critical value, which we determine.**

adhesion | elasticity | stretchable electronics | blistering | buckling

Thin films are adhered to substrates in a range of technological applications either to enhance the mechanical properties of bulk materials or to give the surface novel properties (1). Traditionally, the buckling and delamination of these thin coatings have been viewed as an inconvenience with research focusing on how they might be avoided. More recently, however, both the wrinkling and delamination of such films under compression have been exploited in the development of “flexible electronic” devices (2–7). The goal for these systems is to develop electronic circuits on flexible circuit boards ultimately leading to the manufacture of, among other things, flexible displays and electronic paper (8–10). A major technological challenge limiting the development of such devices is the requirement that the substrate be able to flex without stretching and damaging the wires that make up the circuit. One way to overcome this challenge is to use a polymer substrate that is first stretched and then coated with wires according to the required pattern. On releasing the strain in the substrate, the wires are relatively stiff in compression and so buckle out of the plane to accommodate the imposed deformation. This leads first to a well-studied wrinkling instability (7, 11) and subsequently to the formation of delamination “blisters” (12): localized regions where the film and substrate are no longer bonded. Once formed, these blisters facilitate the flexion of the substrate because the wires can accommodate deformation by bending rather than stretching.

Here, we focus on the features of delamination by characterizing the relationship between the blisters’ size and the material properties and their evolution. This complements the many earlier studies, which only considered the wavelength of the wrinkling instability observed prior to delamination (11, 13, 14) and the appearance of localized structures without delamination (15).

Practical applications of delamination are typically found at a microscopic scale, as for circuitry in flexible electronics (3) mentioned above. However, one unique aspect of our work is that

we perform well-controlled experiments at a larger (macroscopic) scale. This enables us to readily vary and control the material properties of the system over a wider range than would have been possible at a microscopic scale. The underlying physics may nevertheless be equally applied at microscopic scales. In our experiments, a thin Bi-oriented Polypropylene film (with thicknesses  $h$  in the range  $15 \leq h \leq 90 \mu\text{m}$ ) is adhered by van der Waal’s forces to a soft polymeric substrate (Vinylpolysiloxane). We use both thin substrates (which are stretched prior to adhesion) and deep substrates (which are unstretched). Relative to this initial state, the substrate is then uniaxially compressed in a linear stage. For the adhered thin film, however, compression is energetically expensive compared with bending. Therefore, above a critical value of substrate compression the thin film wrinkles with a well-defined wavelength (7, 11). Under further compression wrinkling becomes unstable: the thin film locally debonds and buckles further out of plane.

## Results

We observe that delamination occurs first with the appearance of a single blister. On further compression, a series of approximately identical blisters appear sequentially. The size of these blisters is typically much larger than the wavelength of the wrinkling instability that precedes it. A representative photograph of such an array of delamination blisters generated in our apparatus is shown in Fig. 1A. More details of the experimental procedure are given in *Materials and Methods*.

Our investigation is twofold because we focus on understanding both the characteristic dimensions of the first blister at the onset of delamination and the evolution of multiple blisters between delamination events. Consequently, we performed two different types of experiments. First, we measured the width of the first blister at onset  $\lambda_c$  as a function of the material properties of the system. Second, we measured (using an inclined laser sheet) the evolution of the height profile of the blisters as the compression is increased beyond onset. A schematic diagram of this arrangement is presented in Fig. 1B. Representative (plan view) photographs before and after the onset of delamination for a 90- $\mu\text{m}$ -thick strip are shown in Fig. 1C. From these images, we extract the height profile of the strip, a typical example of which is shown in Fig. 1D. This profile is well approximated by a cosine form,

$$y = d(x) \equiv \frac{\delta}{2} \left[ 1 + \cos \frac{2\pi x}{\lambda} \right], \quad [1]$$

where  $\delta$  and  $\lambda$  are the height and width of the blister, respectively. The form in Eq. 1 is that expected for the buckling of an Euler column for small deformations (16, 17). This allows for  $\delta$  and  $\lambda$  to be readily determined by fitting of the experimental profiles.

Author contributions: B.R. and P.M.R. designed research; D.V., J.B., A.B., and P.M.R. performed research; D.V. and P.M.R. analyzed data; and D.V. and P.M.R. wrote the paper.

The authors declare no conflict of interest.

This article is a PNAS Direct Submission.

See Commentary on page 10875.

<sup>1</sup>To whom correspondence should be addressed. E-mail: preis@mit.edu.

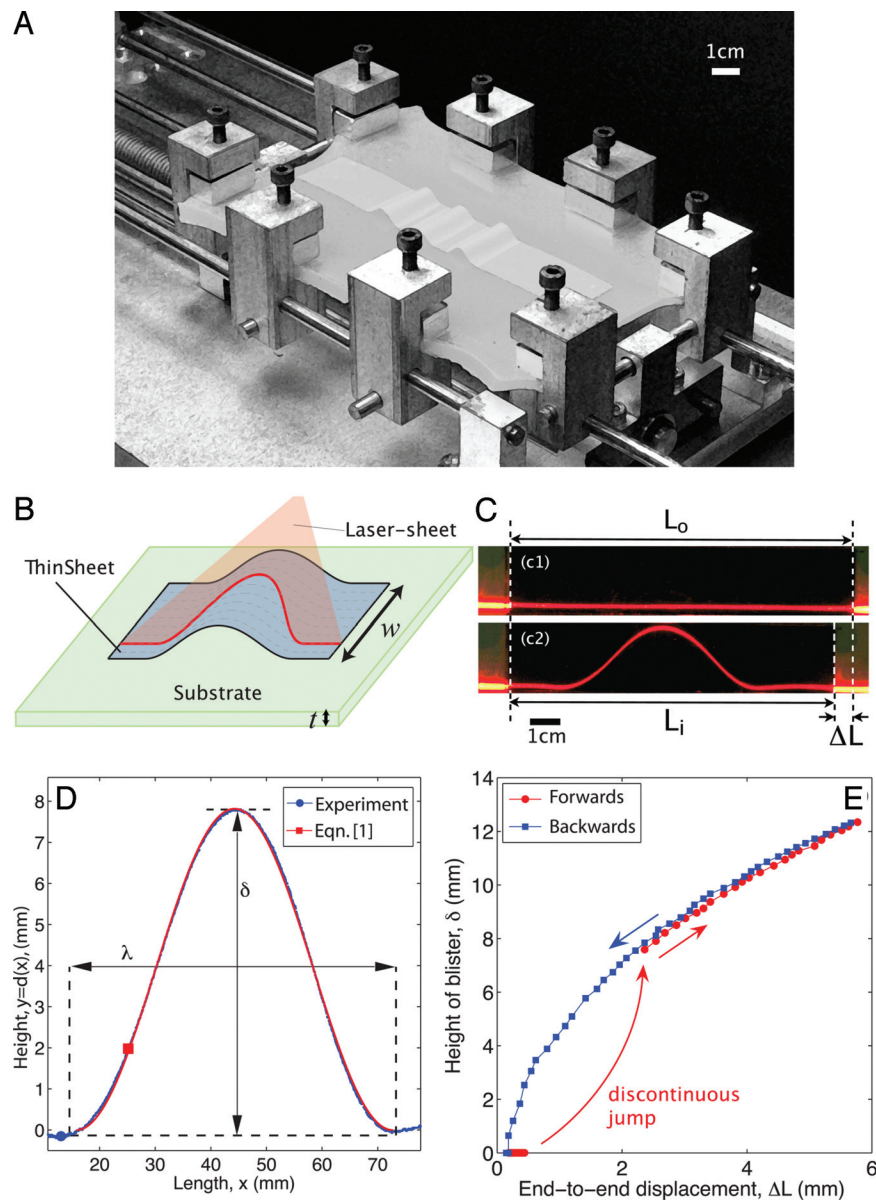


**Fig. 1.** Macroscopic delamination blisters. (A) Macroscopic experimental setup for studying the delamination of thin films adhered to soft substrates. (B) A laser sheet is used to measure the profile of the blister(s) as the end-to-end compression  $\Delta L$  is increased. (C) Plan views of the blister profile as shown by an oblique laser sheet just before (c1) and just after (c2) delamination. (D) Processing these images gives the blister profile  $y = d(x)$  (blue points), which is well fitted by the cosine form Eq. 1 (red curve). This fit gives the blister size  $\lambda$  and height  $\delta$ . (E) Plot of the evolution of the blister height as  $\Delta L$  is increased (red curve) and then decreased (blue curve). In A the film has thickness  $h = 50 \mu\text{m}$ , whereas for C–E,  $h = 90 \mu\text{m}$ .

Our analysis is presented in terms of the end-to-end displacement  $\Delta L = L_o - L_i$ , where  $L_o$  is the total uncompressed length of the flat strip and  $L_i$  is the distance from the left to the right edge of the strip once compression is applied (see Fig. 1C). In our experiment, the total end-to-end displacement of the substrate is controlled, not  $\Delta L$  itself. However, we treat  $\Delta L$  as an imposed control parameter,\* which is measurable directly in experiments. To illustrate the evolution of blister dimensions as  $\Delta L$  increases, Fig. 1E shows the dependence of the height of the blister  $\delta$  on  $\Delta L$ . Under compression of the substrate, the sheet initially remains approximately flat up to a point where both  $\delta$  and  $\Delta L$  change sharply. This discontinuous jump corresponds to the delamination of the strip from the

substrate: a blister forms. On increasing the compression  $\Delta L$  further, the height of the blister also increases. When the compression  $\Delta L$  is subsequently decreased,  $\delta$  decreases smoothly following the previous path. However, the blister persists beyond the compression at which it first appeared, disappearing only once  $\Delta L \approx 0$ . In what follows we do not discuss this hysteretic behavior but believe that it would be of interest to study this further in future work. Henceforth, we will focus on the onset and evolution of blisters under compression only.

An alternative way to represent the evolution of the blister profile is to construct a space-compression diagram in which the strip height profiles  $d(x)$  of the center line of the strip are stacked as a function of  $\Delta L$ . Two representative examples of such diagrams are given in Fig. 2A and B for sheets of thickness  $h = 90 \mu\text{m}$  and  $h = 30 \mu\text{m}$ , respectively. In these diagrams, the color represents the height at each point  $x$  along the center line of the strip for a given value of  $\Delta L$ . In Fig. 2A the value of  $\Delta L$  at

\* A balance-of-forces argument applied at the edge of the sheet perpendicular to the compression direction shows that  $\Delta L$  is directly related to the globally imposed end-to-end displacement.

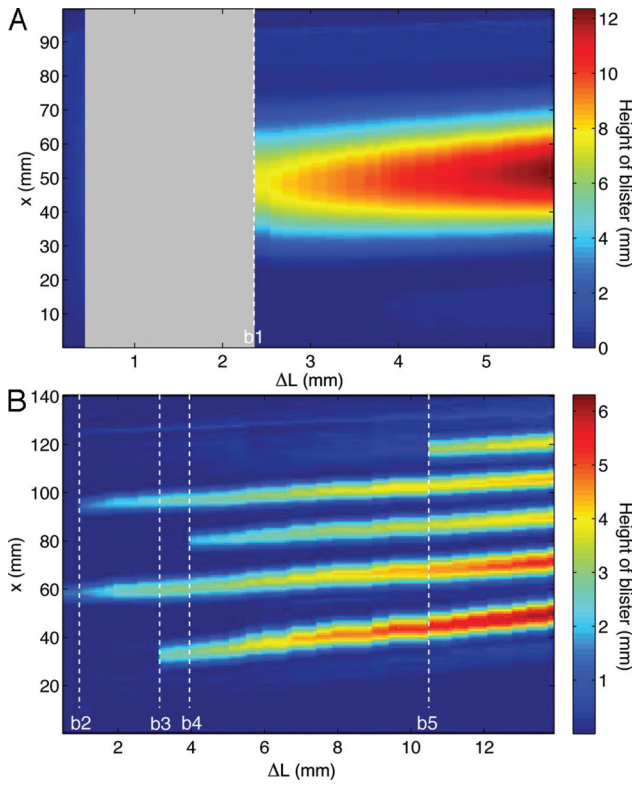


**Fig. 2.** Space-compression plots. Evolution of the blister profile as the end-to-end compression is increased. Color represents the blister height profile shown in the adjacent color bars. A single blister (with  $h = 90 \mu\text{m}$ ) (A) and appearance and evolution of multiple blisters (with  $h = 30 \mu\text{m}$ ) (B). The gray region emphasizes the discontinuity in  $\Delta L$  at the first delamination event.

which the single blister appears is indicated by the vertical dashed line  $b1$ . Note that there are values of  $\Delta L$  through which the system does not pass (gray region). This corresponds to the discontinuity in  $\Delta L$  at delamination, which can also be seen in the “forwards” curve in Fig. 1E. If the compression is increased sufficiently, a series of approximately identical blisters are generated sequentially. A space-compression plot with successive delamination events is shown in Fig. 2B with the appearance of four further blisters indicated by the vertical dashed lines  $b2$ ,  $b3$ ,  $b4$ , and  $b5$ , respectively.

**Blisters at Onset.** We now follow an energetical approach to develop a scaling law for the size  $\lambda_c$  of the blisters at onset as a function of the material properties. The elastic energy of the system is  $\mathcal{U} = \mathcal{U}_b + \mathcal{U}_e$ , where  $\mathcal{U}_b$  is the contribution due to bending of the thin film and  $\mathcal{U}_e$  is the elastic energy of the substrate, which is localized directly underneath the blisters since this is where compression is least restricted. We neglect any compression of the relatively stiff thin film. For a strip of width  $w$  and bending stiffness  $B$ , the bending energy caused by the presence of a single blister is  $\mathcal{U}_b = 1/2Bw \int_{-\lambda/2}^{\lambda/2} d''(x)^2 dx = \pi^4 Bw\delta^2/\lambda^3$ , where  $d''(x)$  is the second derivative with respect to  $x$  of the blister profile given in Eq. 1. The elastic energy stored in the substrate  $\mathcal{U}_e$  depends on the strain  $\epsilon$  accommodated beneath each blister, the substrate elastic modulus  $E_s$  and the substrate thickness  $t$ . We estimate  $\mathcal{U}_e$  in two relevant limiting regimes: (a) large blisters ( $\lambda \gg w, t$ ) and (b) small blisters ( $\lambda \ll w, t$ ). Intermediate regimes may be considered with similar arguments but complicate the subsequent analysis unnecessarily. In each of these limits the volume over which substrate deformation occurs (schematic presented in Figures 3A and B, respectively) scales as the area  $\lambda^2$ , multiplied either by (a) the thickness of the substrate  $t$  or (b) the width of the strip,  $w$ . The

substrate energy density in each case is  $E_s\epsilon^2/2$  so that the energy is  $\mathcal{U}_e = \alpha E_s\epsilon^2\lambda^2$  with  $\alpha \sim t$  for large blisters and  $\alpha \sim w$  for small blisters. The total elastic energy for  $n$  identical blisters is therefore given by

$$\mathcal{U} = n \left( \pi^4 B \frac{\delta^2}{\lambda^3} w + \alpha E_s \epsilon^2 \lambda^2 \right), \quad [2]$$

where the unknown parameters are the number of blisters  $n$ , their width  $\lambda$ , height  $\delta$ , and the strain  $\epsilon$  accommodated by each of them. Using the blister profile given in Eq. 1, we obtain the geometrical relationship

$$\frac{\Delta L}{n} = \frac{\pi^2 \delta^2}{4 \lambda}, \quad [3]$$

which may be used to eliminate  $\delta$  from Eq. 2 in favor of  $\Delta L$ . Also, the strain accommodated by each blister is  $\epsilon = \Delta L/n\lambda$ . Because  $\Delta L$  is treated as a control parameter, the two unknowns are then the blister width  $\lambda$  and the number of blisters  $n$ . If we require that the energy release rate  $-\partial\mathcal{U}/\partial\lambda = n w \Delta\gamma$ , where  $\Delta\gamma$  is the interfacial toughness (16, 18), we find

$$\lambda = 2(\pi\ell_{ec})^{2/3} \left( \frac{\Delta L}{n} \right)^{1/3}, \quad [4]$$

where  $\ell_{ec} \equiv (B/\Delta\gamma)^{1/2}$  is a characteristic length that balances bending and adhesion. This length is directly analogous to the elasto-capillary length in the aggregation of wet hairs (19, 20) where surface tension replaces interfacial toughness. We note that Eq. 4 for a single blister ( $n = 1$ ) was also given by Kendall (21) for a dislocation between an adhering flexible sheet and a rigid substrate. Given a fixed number of blisters, Eq. 4 governs the evolution of the blister size. However, for the apparition of the blistering pattern in the first place, the value of  $n$  is also unknown. Minimizing the elastic energy with respect to variations in  $n$ ,<sup>†</sup> we find that there is a critical value of  $\Delta L/n$  at onset

$$\frac{\Delta L_c}{n} \sim \left( \frac{B\Delta\gamma^2 w^3}{\alpha^3 E_s^3} \right)^{1/5}. \quad [5]$$

Since  $\Delta L$  is increasing in our (displacement-controlled) experiments, blistering first manifests itself with  $n = 1$ . Furthermore, this finite value of  $\Delta L$  at onset explains the jump in  $\Delta L$  observed at delamination (see Figs. 1E and 2A). The threshold blister size,  $\lambda_c$ , is now found by substituting the critical value of  $\Delta L/n$  into Eq. 4. For large blisters ( $\lambda_c \gg w, t$ ) we find

$$\lambda_c \sim \left( \frac{B^2 w}{E_s t \Delta\gamma} \right)^{1/5}, \quad [6]$$

whereas for small blisters ( $\lambda_c \ll w, t$ ) we find

$$\lambda_c \sim \left( \frac{B^2}{E_s \Delta\gamma} \right)^{1/5}. \quad [7]$$

Experimental tests of the predictions Eqs. 6 and 7 are shown in Fig. 3A and B, respectively. The raw data (for  $\lambda_c$  vs.  $w$ ) are provided in Fig. 3A and B Insets. The experimental results are in excellent agreement with the above scalings (dashed lines in Fig. 3). In particular, we note that large blisters,  $\lambda_c \gg w, t$ , follow the  $\lambda_c \sim w^{1/5}$  scaling expected, whereas for small blisters,  $\lambda_c \ll w, t$ ,  $\lambda_c$  is approximately independent of  $w$ . Furthermore, we observe that the rescalings suggested by our analysis yield a good collapse of our data onto a master curve over a wide range of material parameters. Note that our analysis is only valid if the thin film

<sup>†</sup> We assume here that  $n$  is chosen to minimize the elastic energy, although the final result may also be obtained by assuming that it is the strain accommodated by each blister,  $\epsilon$ , that is chosen to minimize the elastic energy.

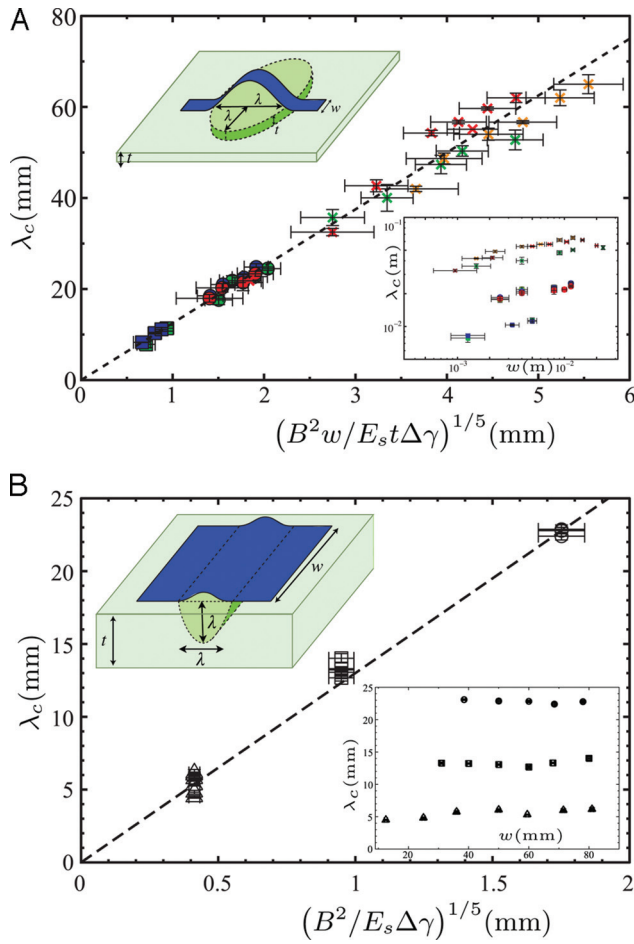


**Fig. 3.** Dimensions of blisters at onset in the two limits considered:  $\lambda \gg w, t$  (A) and  $\lambda \ll w, t$  (B). In each figure, *Insets, Upper left*, show schematic diagrams of the extent of the strained region in the substrate beneath a blister. *Insets, Lower right*, show raw data for  $\lambda_c$  as a function of  $w$ . (A) The blister size  $\lambda_c$  at the onset of delamination for the case of large blisters ( $\lambda \gg w, t$ ) as a function of the scaling prediction in Eq. 6. Data are presented for a range of substrate stretching stiffnesses  $E_s t$  and film thicknesses  $h$ . The substrate stretching stiffnesses are as follows:  $E_s t = 2,200$  N/m (red points),  $E_s t = 1,200$  N/m (blue points),  $E_s t = 800$  N/m (green points), and  $E_s t = 220$  N/m (orange points). The strip thicknesses used are as follows:  $h = 30 \mu\text{m}$  (■),  $h = 50 \mu\text{m}$  (●), and  $h = 90 \mu\text{m}$  (×). (B) The blister size,  $\lambda_c$ , at the onset of delamination for the case of small blisters ( $\lambda \ll w, t$ ) as a function of the scaling prediction in Eq. 7. Data are presented for three different strip thickness  $h$ :  $h = 15 \mu\text{m}$  (▲),  $h = 30 \mu\text{m}$  (■), and  $h = 50 \mu\text{m}$  (●). In these experiments  $E_s \approx 0.22$  MPa and  $t = 5$  cm. Vertical error bars are given by the standard error of 5 repeated experiments.

is incompressible compared with the substrate. For large blisters this requires that  $Eh \gg E_s t$  but for small blisters the condition is  $Eh \gg E_s \lambda$ . In our experiments these inequalities were satisfied by a factor of at least 20 and more typically 100.

**Evolution of Blisters.** We have already observed that the blisters appear sequentially. In between each of these delamination events we see, e.g., Fig. 2, that the blister size  $\lambda$  and height  $\delta$  evolve as the end-to-end compression,  $\Delta L$ , increases. We expect that, with  $n$  fixed,  $\lambda$  should be governed by Eq. 4, or, after using Eq. 3,

$$\delta = \frac{2^{3/2}}{\pi^{2/3}} \ell_{ec}^{1/3} \left( \frac{\Delta L}{n} \right)^{2/3}. \quad [8]$$

We emphasize that Eqs. 4 and 8 depend only on the end-to-end displacement *per blister*,  $\Delta L/n$ . Thus, these relationships are equally valid for a single blister,  $n = 1$ , and for identical

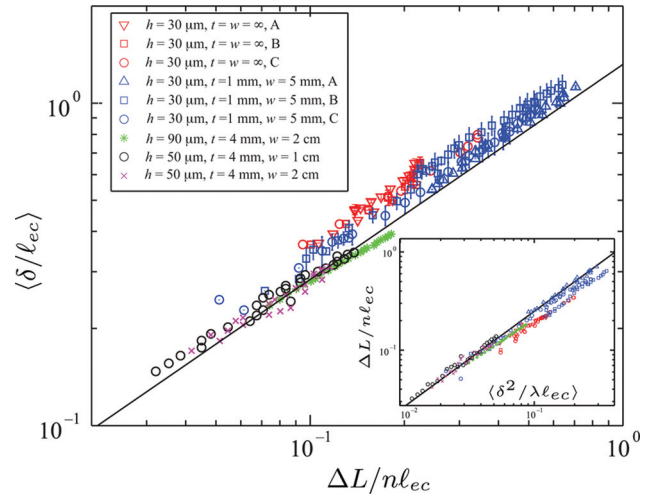


**Fig. 4.** The evolution of the mean blister height ( $\delta$ ) as the end-to-end displacement  $\Delta L$  is increased. Experimental results (points) are shown for a variety of different film thicknesses and widths and for different values of the substrate properties. The solid line shows the theoretical prediction Eq. 8, which has no adjustable parameters. (*Inset*) Experimental measurements of the blister geometry (points) compare well with the theoretical prediction Eq. 3 (line).  $\langle \cdot \rangle$  denotes the average over multiple blisters (here, results are presented for up to 5 blisters) and error bars show the standard error in this average. Points with no error bars correspond to single blisters.

multiple blisters,  $n > 1$ . Fig. 4 shows experimental measurements of the mean blister height,  $\langle \delta \rangle$ , as a function of  $\Delta L/n$  for a range of different material properties and with different numbers of blisters. Plotting the results in this way allows a direct comparison of the evolution of single and multiple blisters with the theoretical prediction in Eq. 8. The agreement between Eq. 8 and the experimental results is striking because there are no adjustable parameters in our model. We also note that the geometrical relationship of Eq. 3 is well satisfied for an arbitrary number of blisters (Fig. 4 *Inset*). However, the experimental values of  $\delta$  are slightly above our predictions. We speculate that this slight discrepancy may be ascribed to the softness of the substrate: the film induces a dip in the surface of the substrate in the region of the contact between film and substrate (25).

## Discussion and Conclusions

Having validated our theoretical formalism with macroscopic experiments, we conclude by considering its application to the microscopic situations relevant for a wide range of technological applications.

**Measuring the Interfacial Toughness.** We note that the interfacial toughness  $\Delta \gamma$  can be simply expressed in terms of the height and width of the blister by eliminating  $\Delta L$  between Eqs. 8 and 4:

$$\Delta \gamma = 2\pi^4 \frac{B\delta^2}{\lambda^4}. \quad [9]$$

Hence,  $\Delta \gamma$  can be easily estimated if the value of the bending stiffness  $B$  is known along with the blister profile, in particular, the values of  $\lambda$  and  $\delta$ . In the delamination of thin metal films— $h = O(100$  nm)—from polymeric substrates under compression  $B$  is known and the blister dimensions— $\lambda = O(10 \mu\text{m})$  and height  $\delta = O(1 \mu\text{m})$ —are typically measured by atomic force microscopy. However, the value of the interfacial toughness  $\Delta \gamma$  is much more difficult to determine (18, 26, 27). In Table 1 we provide a survey of the relevant parameters from several studies of straight-sided blisters in the literature (22–24). By substituting these values into Eq. 9 we are able to estimate the interfacial toughness for each of those cases (Table 1, last column). Our estimated values are in

**Table 1. Typical values from the literature for the properties of blisters and the associated estimate of the interfacial toughness  $\Delta\gamma$** 

Reference	Thin film type	$h$ , nm	$\delta$ , nm	$\lambda$ , $\mu\text{m}$	$\Delta\gamma(\text{Jm}^{-2})$
Cleymand et al. (22)	Stainless steel	58	250	2.3	1.3
Parry et al. (23)	Nickel	50	250	3.5	0.2
Foucher (24)	Nickel	100	340	3.4	3
Foucher (24)	Nickel	200	670	8.9	2
Foucher (24)	Nickel	300	1,000	12.8	3.7

These experiments were all performed on polycarbonate substrates.

reasonable agreement with values determined in similar systems via alternative methods (27, 28). We note, in particular, that in the experiments of Foucher (24) only the film thickness was varied and we therefore expect that the estimates of  $\Delta\gamma$  should be mutually consistent, as is indeed the case.

**Implications for Stretchable Electronics.** We conclude by highlighting some of the implications of our work for stretchable electronics, the technological application that motivated our study. First, we note that the film-substrate system produces blisters with an intrinsic size. This is important for experiments using predefined adhesion patterns (3) because the presence of an intrinsic length scale may lead to the appearance of defects in imposed patterns with different length scales. Indeed, Sun et al. (3) found empirically that the highly adhesive patch of their substrate patterning should be narrower than some critical width to avoid the formation of unwanted delamination blisters (see ref. 3, figure S1). Our formalism can be used to predict this critical size in terms of the mechanical properties of the system. Moreover, the microfabrication process could be simplified significantly by tuning the material properties to produce blisters of a given size, removing the need to selectively alter the substrate adhesion.

In applications of flexible electronics, it is vital that the device retains its mechanical and electrical integrity during repeated use (29). In particular, the buckled wires in these devices should not deform plastically or fracture because this would compromise their conducting characteristics. There are two possible routes to minimize such effects. One is to appropriately choose the material properties of the mechanical system so that buckling does not cause damage. Alternatively, more complex design strategies, for example, multilayer neutral mechanical plane designs (4), can be employed. We consider the former possibility here and show that a simple design criterion could be used in delamination-based devices (3) to avoid irreversible deformation. For this, we assume that irreversible deformations occur when the stress reaches a critical value,  $\sigma_\infty$ —the yield stress. In linear elasticity theory the maximum stress in a deformed sheet is proportional to both the thickness of the sheet and its curvature (30). Requiring this maximum stress to be smaller than  $\sigma_\infty$  we find that

$$\sigma_\infty > \pi^2 \frac{Eh}{1-\nu^2} \frac{\delta}{\lambda^2} = 2^{-1/2} \frac{E}{1-\nu^2} \frac{h}{\ell_{ec}}, \quad [10]$$

where  $E$  is the Young's modulus of the film and  $\nu$  is its Poisson ratio. For a given material, this requires that the thickness be greater than a critical value

$$h > h_c \equiv 6 \frac{E\Delta\gamma}{\sigma_\infty^2(1-\nu^2)} = 6 \frac{\Delta\gamma}{E\epsilon_\infty^2(1-\nu^2)}, \quad [11]$$

where  $\epsilon_\infty = \sigma_\infty/E$  is the yield strain of the film. This safety requirement is independent of the degree of compression and it applies equally well to multiple blisters far beyond onset as it does to a single blister just beyond the blistering threshold. For the films used in our experiments, we measured  $\sigma_\infty = 14 \pm 3 \text{ MPa}$  giving  $h_c = 27 \pm 12 \mu\text{m}$ . This estimate is consistent with our observations that only the thinnest films

( $h = 15 \mu\text{m}$ ) used in our experiments undergo irreversible deformations.

For thin metal films, the critical thickness in Eq. 11 is at least 100 nm and, more typically, 10  $\mu\text{m}$ . These relatively large critical values explain why cracking has been observed in some microscopic experimental realisations (24, 31), while also suggesting that plastic deformation may have occurred in others. With films made from other materials, however, it may be possible to make use of significantly thinner sheets without risking irreversible deformations. For example, using typical values for silicon we find  $h_c \approx 10 \text{ nm}$ . Assuming that the strength of ultrathin graphite films is comparable with the extremely high strength of monolayer graphene sheets (32), our analysis yields  $h_c \approx 0.5 \text{ nm}$ , which corresponds to one or two atomic thicknesses [Recent experiments have shown that the deformation of ultrathin graphite films down to thicknesses of as few as 8 atomic layers are well described by continuum elasticity theory (34).] Recently, there has been significant progress in developing techniques for uniform film deposition (33) and transfer onto arbitrary substrates (35). From a mechanical point of view, these advances along with a small critical thickness  $h_c$  suggest that ultrathin and high-strength films, such as graphene sheets, may be the ideal material for applications of bendable circuitry at small scales using delamination structures. Moreover, there is potential for further improvement on the robustness of devices by combining the criterion for material properties that we have proposed with more advanced multilayer designs (4).

## Materials and Methods

**General.** Biaxially oriented polypropylene sheets (Innovia Films) with thicknesses  $h = 15, 30, 50$ , and  $90 \mu\text{m}$  were used. The rectangular strips had widths in the range  $1 \text{ mm} \leq w \leq 25 \text{ mm}$ . Experiments with strips of different length  $\ell$  showed that the onset blister size was not significantly altered provided that the length is greater than  $\lambda_c$ . For all experiments reported here  $\ell > 2\lambda_c$ .

Polymer substrates were made from Vinylpolysiloxane (Zhermack). Two different polymer melts were used: pink (8 Shore A) and green (22 Shore A). In general, the Young's moduli of these materials were  $E_s \approx 220 \text{ kPa}$  and  $E_g \approx 800 \text{ kPa}$ , respectively though variations were accounted for by direct measurements (see: Measurement of material properties).

For deep substrates we compress uniaxially starting from the undeformed state. For thin substrates, this would produce buckling of the substrate and so we instead first stretch the substrate (uniaxially), adhere the strip to the substrate, and then release the strain gradually. Within the theory of linear elasticity, this is equivalent to a compression relative to the stretched state.

**Blister Profile Measurements.** The blister width at the onset of delamination  $\lambda_c$  was measured from digital photographs (taken from above) by using ImageJ. To measure the evolution of  $\lambda$  and  $\delta$  as the compression  $\Delta L$  is varied, the thin films were painted black. (Measurements of  $\lambda_c$  using this method were consistent with those obtained using the first method confirming that painting has little effect on the material properties of the film.) A laser sheet at an oblique angle was then used to highlight the deflection of the blister and digital photographs were taken from above. Image analysis software, based on the MATLAB image processing toolbox, was written in-house and used to extract the blister profile,  $d(x)$ . The maximum of this profile gives the blister height  $\delta$ . Denoting the two values of  $x$ , where  $d(x) = \delta/2$ , as  $x_1$  and  $x_2$ , we define the blister size by  $\lambda = 2|x_1 - x_2|$  (i.e., double the width at half-maximum), which is consistent with the natural definition of  $\lambda$  because of the sinusoidal blister profile in Eq. 1. However, this is a more robust and reproducible method of measuring  $\lambda$  than measuring the point of contact of the film with the substrate from laser profiles.

**Measurement of Material Properties.** The elastocapillary length,  $\ell_{ec}$ , was measured by clamping one end of the film with an imposed vertical displacement and measuring the extent of de-adhered part of the film. This experiment is the dry adhesion equivalent of the capillary-induced sticking of two hairs (20). In processing our experimental data we use the value of  $\ell_{ec}$ , not  $\Delta\gamma$ . However, for completeness we note that typically the corresponding interfacial toughness is  $\Delta\gamma \approx 0.3 \text{ Jm}^{-2}$ .

The bending rigidity of films was obtained by clamping horizontally one end of each of several strips, and measuring the deflection under their own weight as a function of their length. We deduce bending rigidity by comparing these results with numerical integration of an elastic beam in a gravitational field with the same mass density (measured directly with a precision scale).

The stretching stiffness,  $E_s t$ , of thin substrates was measured by using a dynamometer to measure the force-displacement curve for stretching strains  $<10\%$ . Over this range of strains, the force-displacement curve is linear, allowing the stretching stiffness  $E_s t$  to be determined from the gradient.

- Gioia G, Ortiz M (1997) Delamination of compressed thin films. *Adv Appl Mech* 33:119–192.
- Khang DY, Jiang H, Huang YY, Rogers JA (2006) A stretchable form of single-crystal silicon for high-performance electronics on rubber substrates. *Science* 311:208–212.
- Sun Y, Choi WM, Jiang H, Huang YY, Rogers JA (2006) Controlled buckling of semiconductor nanoribbons for stretchable electronics. *Nat Nanotech* 1:201–207.
- Kim DH, et al. (2008) Stretchable and foldable silicon integrated circuits. *Science* 320:507–511.
- Cao Q, et al. (2008) Medium-scale carbon nanotube thin-film integrated circuits on flexible plastic substrates. *Nature* 454:495–500.
- Ko HC, et al. (2008) A hemispherical electronic eye camera based on compressible silicon optoelectronics. *Nature* 454:748–753.
- Jiang H, Khang DY, Song J, Sun Y, Huang Y, Rogers JA (2007) Finite deformation mechanics in buckled thin films on compliant supports. *Proc Natl Acad Sci USA* 104:15607–15612.
- Chen Y, et al. (2003) Electronic paper: Flexible active-matrix electronic ink display. *Nature* 423:136.
- Forrest SR (2004) The path to ubiquitous and low-cost organic electronic appliances on plastic. *Nature* 428:911–918.
- Rogers JA, et al. (2001) Paper-like electronic displays: Large-area rubber-stamped plastic sheets of electronics and microencapsulated electrophoretic inks. *Proc Natl Acad Sci USA* 98:4835–4840.
- Stafford CM, et al. (2004) A buckling-based metrology for measuring the elastic moduli of polymeric thin films. *Nat Mater* 3:545–550.
- Mei H, Huang R, Chung JY, Stafford CM, Yu HH (2007) Buckling modes of elastic thin films on elastic substrates. *Appl Phys Lett* 90:151902.
- Huang J, et al. (2007) Capillary wrinkling of floating thin polymer films. *Science* 317:650–653.
- Bowden N, Brittain S, Evans AG, Hutchinson JW, Whitesides GM (1998) Spontaneous formation of ordered structures in thin films of metals supported on an elastomeric polymer. *Nature* 393:146–149.
- Pocivavsek L, et al. (2008) Stress and fold localization in thin elastic membranes. *Science* 320:912–916.
- Hutchinson JW, Suo Z (1992) Mixed mode cracking in layered materials. *Adv Appl Mech* 29:63–191.
- Audoly B (1998) Stability of straight delamination blisters. *Phys Rev Lett* 83:4124–4127.
- Volinsky AA, Moody NR, Gerberich WW (2002) Interfacial toughness measurements for thin films on substrates. *Acta Mater* 50:441–466.
- Cohen AE, Mahadevan L (2003) Kinks, rings, and rackets in filamentous structures. *Proc Natl Acad Sci USA* 100:12141–12146.
- Bico J, Roman B, Moulin L, Boudaoud A (2004) Elastocapillary coalescence in wet hair. *Nature* 432:690.
- Kendall K (1976) Preparation and properties of rubber dislocations. *Nature* 261:35–36.
- Cleymand F, Coupeau C, Grilhé J (2001) Experimental investigation of the instability of buckling patterns: From straight-sided to wormlike structures. *Scr Mater* 44:2623–2627.
- Parry G, Coupeau C, Colin J, Cimetière A, Grilhé J (2004) Buckling and post-buckling of stressed straight-sided wrinkles: experimental AFM observations of bubbles formation and finite element simulations. *Acta Mater* 52:3959–3966.
- Foucher F (2007) PhD thesis (Université de Poitiers, Poitiers, France).
- Parry G, et al. (2005) Effect of substrate compliance on the global unilateral post-buckling of coatings: AFM observations and finite element calculations. *Acta Mater* 53:441–447.
- Hamm E, Reis P, LeBlanc M, Roman B, Cerda E (2008) Tearing as a test for mechanical characterization of thin adhesive films. *Nat Mater* 7:386–390.
- Gille G, Rau B (1984) Buckling instability and adhesion of carbon layers. *Thin Solid Films* 120:109–121.
- Cordill MJ, Bahr DF, Moody NR, Gerberich WW (2007) Adhesion measurements using telephone cord buckles. *Mater Sci Eng* 443:150–155.
- Someya T (2008) Optics: Electronic eyeballs. *Nature* 454:703–704.
- Mansfield EH (1989) *The Bending and Stretching of Plates* (Cambridge Univ Press, Cambridge, UK).
- Chen Z, Cotterell B, Wang W (2002) The fracture of brittle thin films on compliant substrates in flexible displays. *Eng Fract Mech* 69:597–603.
- Lee C, Wei X, Jysar JW, Hone J (2008) Measurement of the elastic properties and intrinsic strength of monolayer graphene. *Science* 321:385–388.
- Eda G, Fanchini G, Chhowalla M (2008) Large-area ultrathin films of reduced graphene oxide as a transparent and flexible electronic material. *Nat Nanotech* 3:270–274.
- Poot M, van der Zant HSJ (2008) Nanomechanical properties of few-layer graphene membranes. *Appl Phys Lett* 92:063111.
- Kim KS, et al. (2009) Large-scale pattern growth of graphene films for stretchable transparent electrodes. *Nature*, 457:706–710.

**ACKNOWLEDGMENTS.** We thank Lydéric Bocquet and Denis Bartolo for useful discussions. D.V. is supported by the Royal Commission for the Exhibition of 1851. This work was supported in part by European Union New and Emerging Science and Technology project “Mechplant” and by the French ANR-Jeune “MecaWet.”